Acta Crystallographica Section D
Biological Crystallography
ISSN 0907-4449

Structure of human α-enolase (hENO1), a multifunctional glycolytic enzyme

Hyo Jin Kang,[a] Suk-Kyeong Jung,[b] Seung Jun Kim[b]* and Sang J. Chung[a,c]*

[a]BioNanotechnology Research Center, Korea Research Institute of Bioscience and Biotechnology and Division of Nanobiotechnology, Korea University of Science and Technology (UST), Yuseong, Daejeon 305-333, Republic of Korea, [b]Translational Research Center, Korea Research Institute of Bioscience and Biotechnology, Yuseong, Daejeon 305-333, Republic of Korea, and [c]Gachon BioNano Research Institute, Kyungwon University, Seongnam 461-701, Republic of Korea

Correspondence e-mail: ksj@kribb.re.kr, sjchung@kribb.re.kr

Received 31 October 2007
Accepted 31 March 2008

PDB Reference: human α-enolase, 3b97, r3b97sf.

Aside from its enzymatic function in the glycolytic pathway, α-enolase (ENO1) has been implicated in numerous diseases, including metastatic cancer, autoimmune disorders, ischaemia and bacterial infection. The disease-related roles of ENO1 are mostly attributed to its immunogenic capacity, DNA-binding ability and plasmin(ogen) receptor function, which are significantly affected by its three-dimensional structure and surface properties, rather than its enzymatic activity. Here, the crystal structure of human ENO1 (hENO1) is presented at 2.2 Å resolution. Despite its high sequence similarity to other enolases, the hENO1 structure exhibits distinct surface properties, explaining its various activities, including plasmin-(ogen) and DNA binding.

1. Introduction

Enolase, a key enzyme in the glycolytic pathway, is ubiquitously present in a wide range of organisms from bacteria to mammals. Mammals contain three enolase isotypes, denoted α, β and γ. α-Enolase (ENO1) is found in a variety of tissues, while β-enolase (ENO3) is exclusively expressed in muscle tissues and γ-enolase (ENO2) is present in neurons and neuroendocrine tissues (Pancholi, 2001). ENO1 (EC 4.2.1.11) has been the focus of recent research owing to its multifunctional roles in diseases (Gerlt *et al.*, 2005; Kim & Dang, 2005; Glasner *et al.*, 2006; Liu & Shih, 2007) such as cancers (Katayama *et al.*, 2006; Kanemoto *et al.*, 2006; Gruber-Olipitz *et al.*, 2004), autoimmune disorders (Mosca *et al.*, 2006; Weleber *et al.*, 2005; Kinloch *et al.*, 2005; Gitlits *et al.*, 2001), infections (Bergmann *et al.*, 2005; Ehinger *et al.*, 2004) and ischaemia (Anand & Stead, 2005). The disease-related roles of ENO1 mostly rely on its immunogenic properties (Fujii *et al.*, 2005; Yoneda *et al.*, 2007), DNA-binding ability (Al-Giery & Brewer, 1992; Subramanian & Miller, 2000; Wang *et al.*, 2005) and plasmin(ogen) receptor function (Miles *et al.*, 1991; Ehinger *et al.*, 2004; Bergmann *et al.*, 2005).

ENO1 has been identified on the cell surface as well as within the nucleus and cytosol. However, the signal peptides responsible for its localization remain to be identified. ENO1 is highly expressed in tumour cells (Altenberg & Greulich, 2004; Altenberg *et al.*, 2006) and may recruit plasminogen in the tumour environment. Plasminogen bound to the cell surface is converted to plasmin by plasminogen activators and subsequently activates procollagenase to collagenase. This enzyme system is involved in wound healing, tissue remodelling, embryogenesis and cell spreading in the body by degrading fibrin and extracellular matrix (Plow *et al.*, 1995).

The role of ENO1 in tumour-cell invasion and metastasis may be explained by a similar process (Reuning *et al.*, 1998). Enolases on bacterial surfaces participate in the invasion of pathogenic bacteria into tissues, resulting in systemic infection (Bergmann *et al.*, 2005; Plow *et al.*, 1995). These enzymes additionally act as autoantigens to cause encephalopathy (Fujii *et al.*, 2005; Yoneda *et al.*, 2007), retinopathy (Weleber *et al.*, 2005) and rheumatoid arthritis (Kinloch *et al.*, 2005). The DNA-binding ability of ENO1 mainly depends on its *myc* promoter-binding protein-1 (MBP-1) domain (Aoki *et al.*, 2006; Subramanian & Miller, 2000; Feo *et al.*, 2000; Sedoris *et al.*, 2007). MBP-1, an alternative translation product of ENO1 mRNA, binds to the *c-myc* P2 promoter to downregulate *c-myc* expression (Subramanian & Miller, 2000; Feo *et al.*, 2000).

While the crystal structures of bacterial enolases (Ehinger *et al.*, 2004; Hosaka *et al.*, 2003; Giotto *et al.*, 2003), yeast ENO1 (Zhang *et al.*, 1997; Lebioda *et al.*, 1989; Lebioda & Stec, 1988) and human ENO2 (γ-enolase; Chai *et al.*, 2004) have been determined, those of human ENO1 (hENO1) and ENO3 (hENO3) have yet to be solved. To date, most structural analyses have focused on the active sites of the enolases, rather than the features related to DNA binding, plasmin-(ogen) receptor and immunogenic functions, with a few exceptions (Ehinger *et al.*, 2004). Recent reports have described noncatalytic multifunctionality of ENO1 in cancer metastasis, infection and autoimmune diseases (Liu & Shih, 2007; Kim & Dang, 2005; Pancholi, 2001). Here, we resolve the crystal structure of hENO1, which displays surface properties that are distinct from those of other enolases despite high sequence similarity.

2. Materials and methods

2.1. Expression and purification

Human ENO1 cDNA encoding full-length protein (434 amino acids) was a gift from the 21C Human Gene Bank, Genome Research Center, KRIBB, Korea. The forward primer (5′-GGGAATTC**CATATG**TCTATTCTCAAGATC-CATGCC-3′) and reverse primer (5′-CCG**CTCGAG**TTA-CTTGGCCAAGGGGTTTG-3′) were designed based on the hENO1 DNA sequence, with *Nde*I and *Xho*I restriction sites, respectively, shown in bold. Human ENO1 was amplified by PCR using the primers described above and its cDNA as template. The PCR product was digested with *Nde*I and *Xho*I and subcloned into *Nde*I–*Xho*I-digested pET28a(+) vector (Novagen). The resulting N-terminally His-tagged full-length human ENO1 (hENO1) was expressed in *Escherichia coli* Rosetta (DE3) (Novagen). Expression of the His-tagged protein was induced by adding 1 m*M* IPTG at 291 K for 16 h. Cells were harvested by centrifugation at 3570*g* and sonicated in lysis buffer [50 m*M* Tris–HCl pH 7.5, 500 m*M* NaCl, 1 m*M* phenylmethylsulfonyl fluoride, 0.05%(*v*/*v*) β-mercaptoethanol and 5% glycerol]. His-tagged hENO1 was purified by cobalt-affinity chromatography (Clontech). After removal of the His tag by thrombin digestion at 277 K for 20 h, crude hENO1 was purified using Mono Q ion-exchange column chromatography.

Table 1
Data-collection and refinement statistics.

Values in parentheses are for the highest resolution shell.

Data collection	
Space group	$P4_2$
Unit-cell parameters (Å, °)	$a = b = 192.8$, $c = 65.2$, $\alpha = \beta = \gamma = 90$
Resolution (Å)	2.2 (2.28–2.20)
Total reflections	765604
Unique reflections	120965
Completeness (%)	99.5 (97.8)
$R_{\rm merge}$† (%)	8.3 (23.9)
$I/\sigma(I)$	19.6 (6.1)
Refinement	
No. of reflections	118254 [$I \geq 0$]
No. of atoms	
Protein	13196
Heteroatoms	28
Water	617
$R_{\rm cryst}/R_{\rm free}$	19.2/21.4
R.m.s. deviations	
Bond distances (Å)	0.005
Bond angles (°)	1.3
Impropers (°)	0.8
Dihedrals (°)	21.8
Temperature factors (Å^2)	
Protein	23
Heteroatoms	20
Water molecules	24

† $R_{\rm merge} = \sum_{hkl}\sum_i |I_i(hkl) - \langle I(hkl)\rangle| / \sum_{hkl}\sum_i I_i(hkl)$, where $I_i(hkl)$ is the intensity of the ith measurement of an equivalent reflection with indices hkl.

The hENO1 protein was further purified on a Sephacryl S-100 size-exclusion column (Amersham Pharmacia) by eluting in buffer containing 20 m*M* Tris–HCl pH 8.0, 150 m*M* NaCl, 20 m*M* $MgCl_2$, 1 m*M* PMSF and 0.05%(*v*/*v*) β-mercapto-ethanol. Pure hENO1 fractions were combined, concentrated to 20 mg ml^{-1} and used directly for crystallization.

2.2. Crystallization and data collection

Crystallization was performed at room temperature (291 K) using the hanging-drop vapour-diffusion method. Crystals were grown by mixing 1 µl hENO1 solution (20 mg ml^{-1}) and an equal volume of reservoir solution [100 m*M* Tris–HCl pH 7.5 containing 20–24%(*w*/*v*) PEG 3350, 200 m*M* ammonium sulfate and 1 m*M* DTT]. Full-size hENO1 crystals were obtained after 3 d. X-ray diffraction data were collected on beamline 4A at Pohang Accelerator Laboratory (Pohang, Korea) using an ADSC Quantum 4 detector. The crystal diffracted to 2.2 Å resolution and belonged to space group $P4_2$, with unit-cell parameters $a = b = 192.8$, $c = 65.2$ Å, $\alpha = \beta = \gamma = 90^\circ$. The diffraction data collected were processed and scaled with *DENZO* and *SCALEPACK* (Otwinowski & Minor, 1997). Statistics of data collection and refinement are shown in Table 1.

2.3. Structure solution and refinement

The hENO1 structure was determined by the molecular-replacement method using a dimeric human γ-enolase structure (hENO2; PDB code 1te6; Chai *et al.*, 2004) as a search model. The molecular search was performed with *Phaser*

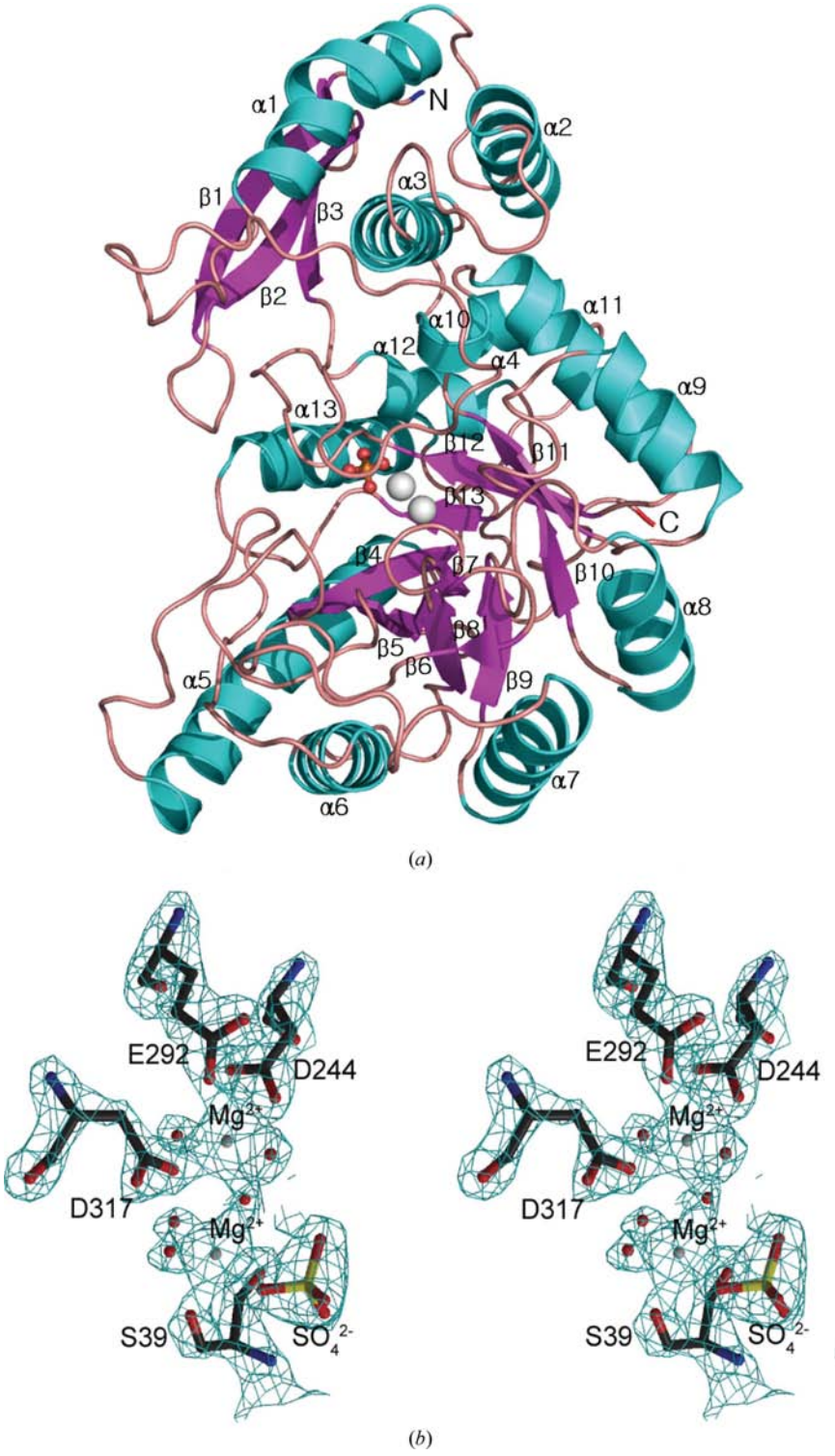

Figure 1
Structure of hENO1. (*a*) Ribbon diagram of hENO1. Secondary-structural elements (helices, cyan; strands, magenta; loops, pink) assigned using *PROCHECK* are labelled. Bound magnesium and sulfate ions are depicted as ball-and-stick models. The boundaries of the secondary-structural elements are as follows: β1, 4–11; β2, 17–25; β3, 28–33; β4, 146–153; β5, 166–170; β6, 240–244; β7, 251–252; β8, 255–256; β9, 288–292; β10, 313–316; β11, 338–341; β12, 365–369; β13, 391–393; α1, 62–78; α2, 86–97; α3, 107–124; α4, 129–137; α5, 177–199; α6, 219–232; α7, 272–285; α8, 300–310; α9, 324–333; α10, 343–346; α11, 349–361; α12, 379–386; α13, 400–416. (*b*) Active site. A difference electron-density map ($F_o - F_c$) around the active site omitted in map calculation was drawn using the refined model. The map was contoured at the 5.0σ level.

(McCoy *et al.*, 2005). The best solution for the first dimer had a log-likelihood gain (LLG) of 1460 and a *Z* score for the translation function (TFZ) of 7275, whereas the best solution for the second dimer reached an LLG of 2062 with a TFZ *Z* score of 10171.

To avoid coupling between the working and test data sets, the test set (5%) for $R_{\rm free}$ calculation was selected from 20 thin shells. The structure was refined using *CNS* (Brünger *et al.*, 1998) with the MLF target, while iterative manual building was performed using *O* (Jones *et al.*, 1991). As the four protomers in the asymmetric unit essentially adopt the same conformation, noncrystallographic symmetry restraints were applied during refinement and were released at the final stage. Water molecules were gradually added during refinement using the water-pick protocol implemented in *CNS* (Brünger *et al.*, 1998). Strong electron densities that were not part of the protein were observed near the active sites of the four protomers. These were modelled as sulfate ions considering the crystallization conditions (Fig. 1*b*). Statistics of data collection and structure refinement are summarized in Table 1. The final $R_{\rm cryst}$ and $R_{\rm free}$ values are 19.2% and 21.4%, respectively. A Ramachandran plot drawn using *PROCHECK* (Laskowski *et al.*, 1993) showed that 87.5% and 12.2% of all residues fell within the most favoured and additionally allowed regions, respectively. There were no residues in the disallowed region. The final model includes residues 1–432 of protomers *A* and *B*, residues 1–433 of protomer *C*, residues 1–431 of protomer *D*, 617 water molecules, eight magnesium ions and four sulfate ions. Fig. 1 was generated using *PyMOL* (http://www.pymol.org), *BOBSCRIPT* (Esnouf, 1997) and *MOLSCRIPT* (Kraulis, 1991).

2.4. Electrostatic potential surface

The surface potentials were calculated and visualized using the program *GRASP*, which contains rapid algorithms for the construction of rendered molecular surfaces and for solution of the Poisson–Boltzmann equation (Nicholls *et al.*, 1991). The electrostatic surface potentials were calculated with contours from $-10kT\,e^{-1}$ (red) to $+10kT\,e^{-1}$ (blue) (where k is Boltzmann's constant and T is temperature). Default

parameters in *GRASP* (exterior dielectric constant of 80, interior dielectric constant of 4, 0.0 *M* ionic concentration) were applied to this calculation. Charges were assigned to each ionisable residue, *i.e.* aspartate, glutamate, lysine and arginine, using the full.crg option as implemented in *GRASP*.

3. Results and discussion

3.1. Overall structure

The structure of hENO1 (Fig. 1*a*) is essentially divided into N-terminal (residues 1–138) and C-terminal (residues 139–432) domains. The N-terminal domain comprises a three-stranded β-sheet with three flanking α-helices, while the C-terminal domain consists of an eightfold β-α barrel. The global structure of hENO1 is markedly similar to that of the prototypical yeast enolase (Zhang *et al.*, 1997; 63.1% sequence identity and 78.8% sequence homology), which has been extensively characterized using biochemical and structural methods. Two types of yeast ENO1 structures have been reported, with 'open' and 'closed' conformations. Accordingly, the refined structure of hENO1 was superimposed on those of the two conformers. Superpositions were performed with the *O* program using a distance criterion of less than 3.8 Å for more than three consecutive C^{α} atoms. When the hENO1 structure was aligned with that of yeast ENO1 with the open conformation (PDB code 1ebh; Wedekind *et al.*, 1995), 410 of 432 C^{α} atoms were superimposed with a root-mean-square deviation of 1.2 Å, whereas alignment with the closed (or complexed) conformation structure (PDB code 1one; Larson *et al.*, 1996) yielded a superposition of 432 C^{α} atoms with a root-mean-square deviation of 0.7 Å. These results imply that hENO1 adopts the closed conformation.

Some enolases show dimeric asymmetry, possibly representing negative cooperativity within the dimer (Chai *et al.*, 2004). However, all the C^{α} atoms of the four protomers in the asymmetric unit were superposed on each other with a root-mean-square deviation of less than 0.5 Å, discounting the possibility of negative cooperativity in hENO1.

Table 2
Comparison of putative plasmin(ogen)-binding sites between bacterial and mammalian enolases and fractional solvent accessibility (FSA).

	Amino-acid residue number in plasmin(ogen)-binding motif†										
Enolase	250	251		252		253	254		255		256
S. pneumoniae	F	Y	D	K	E	–	–	R	K	V	Y
$Eno^{int/del}$‡	F	Y	D	L	G	–	–	R	L	V	Y
Candida albicans	F	Y	–	K	D	A	G	–	K	–	Y
Fasciola hepatica	F	Y	–	K	E	–	G	–	K	–	Y
Rat α	F	Y	–	R	–	A	G	–	K	–	Y
hENO1	F	F	–	R	–	S	G	–	K	–	Y
FSA of hENO1§	0.00	0.26	–	0.34	–	0.97	0.61	–	0.49	–	0.00

† The numbering was based on the amino-acid sequence of hENO1. ‡ $Eno^{int/del}$ is a mutated spENO1 which does not bind to plasminogen. This enzyme was prepared by replacing the two lysine residues in the internal plasminogen-binding motif with leucine as well as replacing Glu with Gly and by truncation of the C-terminal plasminogen-binding domain (Bergmann *et al.*, 2003). § The FSA of each amino acid in the hENO1 structure was calculated using the program *QUANTA* as the ratio of the side-chain fractional solvent accessibility for residue *X* to the fractional solvent accessibility obtained after reducing the structure to a Gly-*X*-Gly tripeptide.

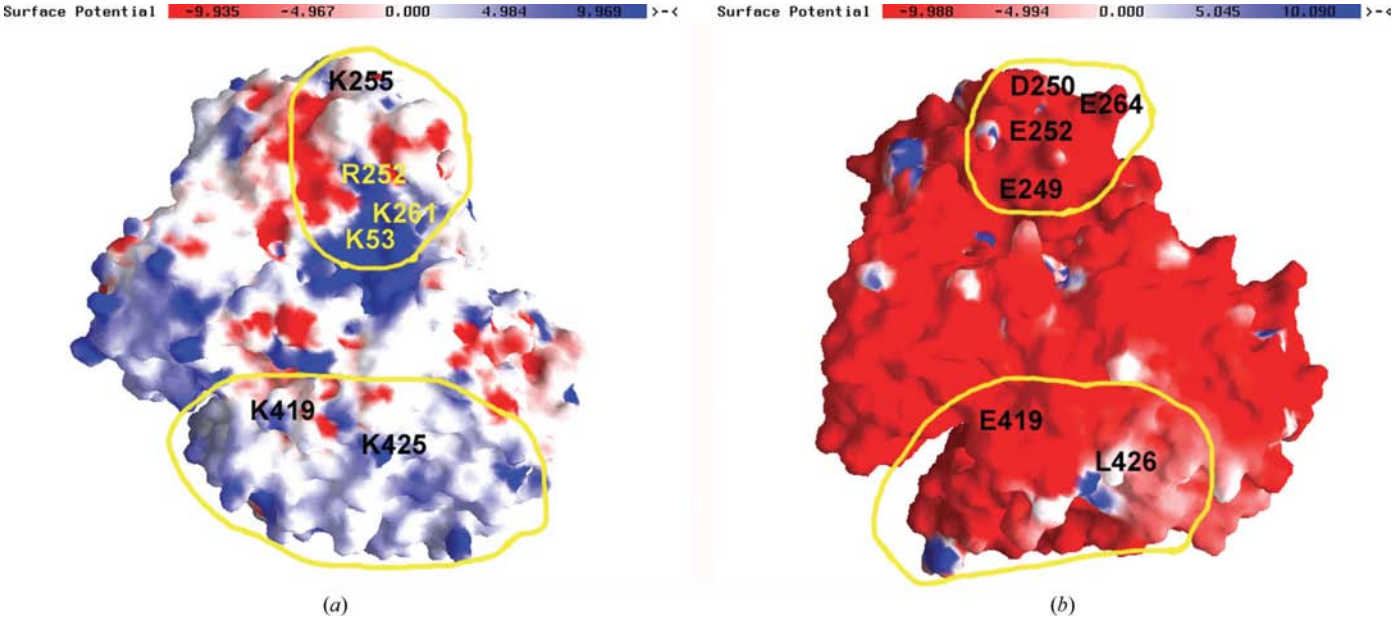

Figure 2
The potential plasmin(ogen)-binding surfaces of hENO1 (*a*) and spENO1 (*b*). The electrostatic potential surfaces of hENO1 and spENO1 are presented using the program *GRASP*. The spENO1 electrostatic surface was derived from the crystallographic coordinates of the *S. pneumoniae* enzyme (PDB code 1w6t). The electrostatic potentials were calculated with contours from $-10kT\ e^{-1}$ (red) to $+10kT\ e^{-1}$ (blue) and with an exterior dielectric constant of 80. Two binding sites with surrounding regions are bordered by yellow lines and several representative residues are labelled.

3.2. Active-site structure

The active site of hENO1 consists of the L1 (residues 36–43), L2 (residues 156–162) and L3 (residues 262–270) loops, two magnesium ions bound to Glu292, Asp317, Asp244 and Ser39, and water molecules (Fig. 1*b*). The common active (or closed) conformation of all enolases can be defined by the surrounding three loops (L1–L3) that encompass the active site, which would be occupied by potential substrates. Upon crystallization of hENO1 without the substrate, hENO1 adopted the closed conformation, which was possibly induced by the sulfate ion bound to the active site. Two magnesium ions and a sulfate ion in the active site were also located at similar positions to the corresponding atoms in the closed structure of yeast enolase (Larson *et al.*, 1996).

3.3. Comparison of the surface of hENO1 with those of other enolases

Both eukaryotic and bacterial α-enolases have the ability to bind plasmin(ogen). To establish the mechanisms of plasmin-(ogen) binding, we generated a surface representation of hENO1 for comparison with that of *Streptococcus pneumoniae* enolase 1 (spENO1; Fig. 2; Ehinger *et al.*, 2004).

The general features of the surface potentials were very different in hENO1 and spENO1. The surface of spENO1 showed a higher degree of negative potential compared with that of hENO1 (Fig. 2). To date, two distinct binding sites have been identified and some similarities exist between the primary sequences of eukaryotic and bacterial α-enolases. One binding site consists of 6–8 residues, including two anti-

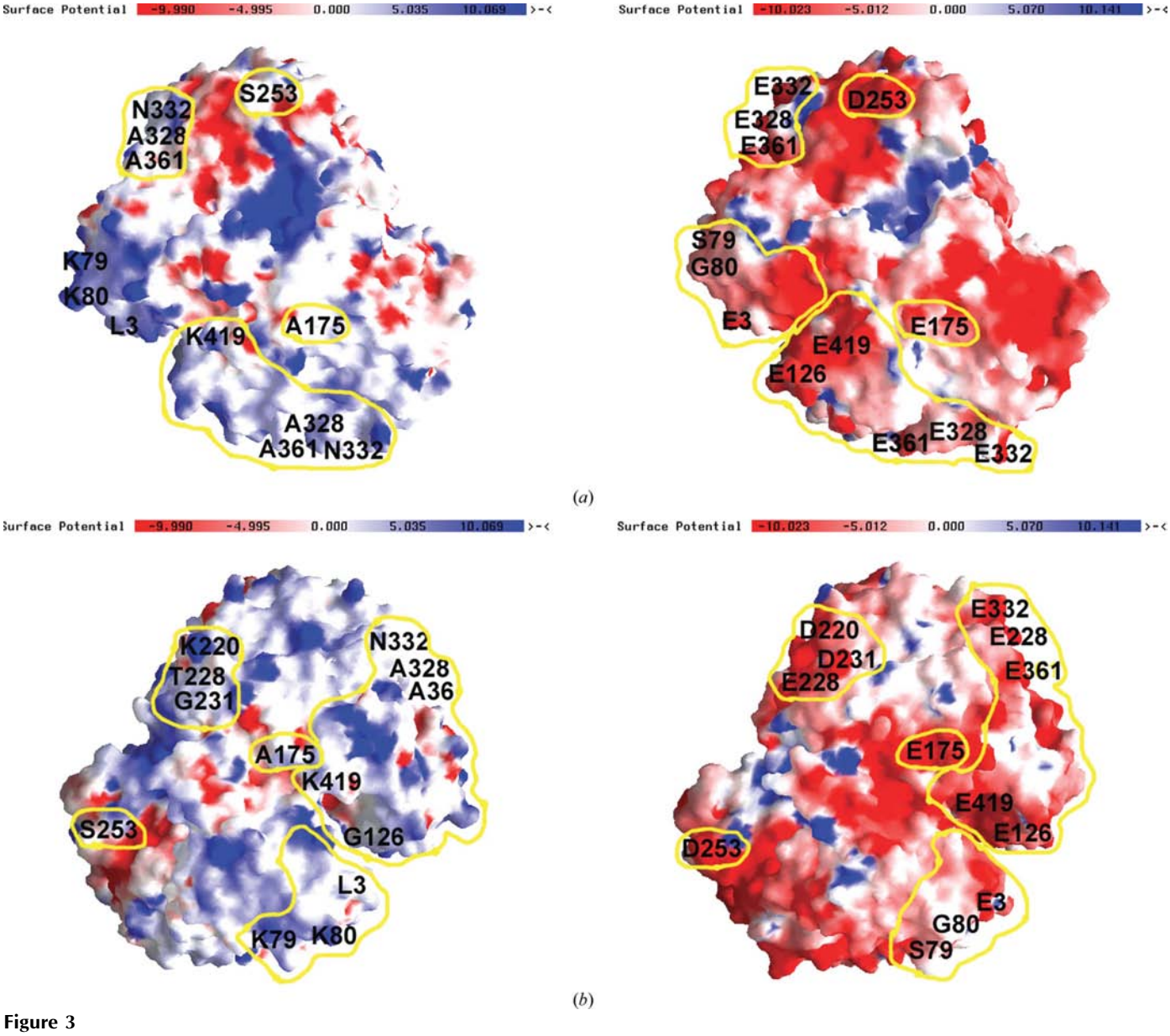

Figure 3
Comparison of electrostatic potentials for hENO1 (*a*) and hENO2 (*b*). Two points of view for each protein are presented, which are rotated by 180° along the *y* axis to each other. The different charged patches are labelled and bordered by solid yellow lines. The same calculation protocols as used in Fig. 2 were applied to this figure.

parallel β-strands (β7 and β8), and the other is located at the C-terminus. The putative plasmin(ogen)-binding motif of hENO1 ($_{250}$FFRSGKY$_{256}$) includes three hydrophobic and two hydrophilic residues. We additionally calculated the side-chain fractional solvent accessibility (FSA) of each residue in the plasminogen-binding motif in order to gain an insight into the residues participating in interactions with other proteins (Table 2).

The side chains of the three hydrophobic residues (Phe250, Phe251 and Tyr256 of hENO1) are completely buried or have only a small fraction exposed (FSA < 0.3; Table 2), whereas the FSA values for the hydrophilic residues range from 0.34 to 0.97. These results imply that the mode of plasmin(ogen) binding is dominated by the polar interactions arising from a possible complementary fit of plasmin(ogen) to the enolase surface as previously reported for spENO1 (Bergmann *et al.*, 2003). Sequence alignment with available enolases shows that the residues within the two antiparallel β-strands (β7 and β8) are variable compared with other regions. Nevertheless, they also show the common features of containing two or three hydrophilic residues as described in a previous review (Pancholi, 2001). At this stage, however, it cannot be excluded that the exact features of the plasminogen-binding site are influenced by conformational changes upon substrate binding. While precise comparisons are hampered by possible weak or disordered electron densities for the putative binding sites in spENO1, the binding site at the C-terminus is apparently blocked by tight octameric association within spENO1 (Ehinger *et al.*, 2004). As hENO1 forms a dimer, however, its C-terminus is exposed to solvent, explaining the distinct binding specificities for plasmin(ogen).

Chai *et al.* (2004) reported that human neuronal-specific enolase (hENO2) has a higher degree of negatively charged surface structure than hENO1 in order to maintain the resting potential of neurons, similar to other neuron-specific proteins. In this investigation, the authors had to rely on a structure of hENO1 generated by molecular modelling to explain the differences in the surface-charge distribution of hENO2 and hENO1. Determination of the crystal structure of hENO1 will facilitate a more reliable comparison. Interestingly, despite high sequence identity (~84%) between the two proteins, the charge distribution on the hENO1 surface is distinct from that of hENO2 (Fig. 3). 11 positively charged residues of hENO1 on the surface are altered to either negatively charged (three) or neutral (eight) residues in hENO2. In addition, ten neutral residues of hENO1 are negatively charged in the neuronal enolase, explaining the higher pI value (7.38) of hENO1 compared with that of hENO2 (4.75). The positively charged surface of hENO1 is possibly related to its noncatalytic function. In particular, in view of its positively charged surface, hENO1 should display a stronger DNA-binding ability than hENO2. Additionally, the distinct surface properties of hENO1 may be responsible for other noncatalytic functions, such as plasmin(ogen) binding and autoantigen activity. Further biological experiments are required to confirm the validity of the above suggestions.

In summary, we have reported the hENO1 structure for the first time. Structural analyses revealed that hENO1 has surface properties that are distinct from those of other enolases despite high sequence identity. The results will afford a structural basis for understanding the multifunctional properties of ENO1. In addition, these results provide a good example of slight sequence diversities in proteins that manifest themselves as distinguishable surface properties which can cause the proteins to display totally different biological functions.

This work was supported by the R&D Program for Fusion Strategy of Advanced Technologies (MOCIE) and the Bio-signal Analysis Technology Innovation Program (M10645010003-06N4501-00310) of the Ministry of Science and Technology (MOST) and the Korea Science and Engineering Foundation (KOSEF).

References

Al-Giery, A. G. & Brewer, J. M. (1992). *Biochim. Biophys. Acta*, **1159**, 134–140.
Altenberg, B., Gemuend, C. & Greulich, K. O. (2006). *Proteomics*, **6**, 67–71.
Altenberg, B. & Greulich, K. O. (2004). *Genomics*, **84**, 1014–1020.
Anand, N. & Stead, L. G. (2005). *Cerebrovasc. Dis.* **20**, 213–219.
Aoki, T., Imamura, T., Ozaki, H., Ideuchi, H., Tsuchida, S. & Watabe, H. (2006). *Biosci. Biotechnol. Biochem.* **70**, 1921–1927.
Bergmann, S., Rohde, M., Preissner, K. T. & Hammerschmidt, S. (2005). *Thromb. Haemost.* **94**, 304–311.
Bergmann, S., Wild, D., Diekmann, O., Frank, R., Bracht, D., Chhatwal, G. S. & Hammerschmidt, S. (2003). *Mol. Microbiol.* **49**, 411–423.
Brünger, A. T., Adams, P. D., Clore, G. M., DeLano, W. L., Gros, P., Grosse-Kunstleve, R. W., Jiang, J.-S., Kuszewski, J., Nilges, M., Pannu, N. S., Read, R. J., Rice, L. M., Simonson, T. & Warren, G. L. (1998). *Acta Cryst.* D**54**, 905–921.
Chai, G., Brewer, J. M., Lovelace, L. L., Aoki, T., Minor, W. & Lebioda, L. (2004). *J. Mol. Biol.* **341**, 1015–1021.
da Silva Giotto, M. T., Hannaert, V., Vertommen, D., de A. S. Navarro, M. V., Rider, M. H., Michels, P. A. M., Garratt, R. C. & Rigden, D. J. (2003). *J. Mol. Biol.* **331**, 653–665.
Ehinger, S., Schubert, W.-D., Bergmann, S., Hammerschmidt, S. & Heinz, D. W. (2004). *J. Mol. Biol.* **343**, 997–1005.
Esnouf, R. M. (1997). *J. Mol. Graph.* **15**, 112–134.
Feo, S., Arcuri, D., Piddini, E., Passantino, R. & Giallongo, A. (2000). *FEBS Lett.* **473**, 47–52.
Fujii, A., Yoneda, M., Ito, T., Yamamura, O., Satomi, S., Higa, H., Kimura, A., Suzuki, M., Yamashita, M., Yuasa, T., Suzuki, H. & Kuriyama, M. (2005). *J. Neuroimmunol.* **162**, 130–136.
Gerlt, J. A., Babbitt, P. C. & Rayment, I. (2005). *Arch. Biochem. Biophys.* **433**, 59–70.
Gitlits, V. M., Toh, B.-H. & Sentry, J. W. (2001). *J. Invest. Med.* **49**, 138–145.
Glasner, M. E., Gerlt, J. A. & Babbitt, P. C. (2006). *Curr. Opin. Chem. Biol.* **10**, 492–497.
Gruber-Olipitz, M., Afjehi-Sadat, L., Felizardo, M., Slavc, I. & Lubec, G. (2004). *Cancer Genomics Proteomics*, **1**, 311–338.
Hosaka, T., Meguro, T., Yamato, I. & Shirakihara, Y. (2003). *J. Biochem.* **133**, 817–823.
Jones, T. A., Zou, J.-Y., Cowan, S. W. & Kjeldgaard, M. (1991). *Acta Cryst.* A**47**, 110–119.
Kanemoto, K., Satoh, H., Ishikawa, H. & Sekizawa, K. (2006). *Clin. Oncol. (R. Coll. Radiol.)*, **18**, 505.

Katayama, M., Nakano, H., Ishiuchi, A., Wu, W., Oshima, R., Sakurai, J., Nishikawa, H., Yamaguchi, S. & Otsubo, T. (2006). *Surg. Today*, **36**, 1085–1093.
Kim, J.-W. & Dang, C. V. (2005). *Trends Biochem. Sci.* **30**, 142–150.
Kinloch, A., Tatzer, V., Wait, R., Peston, D., Lundberg, K., Donatien, P., Moyes, D., Taylor, P. C. & Venables, P. J. (2005). *Arthritis Res. Ther.* **7**, R1421–R1429.
Kraulis, P. J. (1991). *J. Appl. Cryst.* **24**, 946–950.
Larson, T. M., Wedekind, J. E., Rayment, I. & Reed, G. H. (1996). *Biochemistry*, **35**, 4349–4358.
Laskowski, R. A., MacArthur, M. W., Moss, D. S. & Thornton, J. M. (1993). *J. Appl. Cryst.* **26**, 283–291.
Lebioda, L. & Stec, B. (1988). *Nature (London)*, **333**, 683–686.
Lebioda, L., Stec, B. & Brewer, J. M. (1989). *J. Biol. Chem.* **264**, 3685–3693.
Liu, K.-J. & Shih, N.-Y. (2007). *J. Cancer Mol.* **3**, 45–48.
McCoy, A. J., Grosse-Kunstleve, R. W., Storoni, L. C. & Read, R. J. (2005). *Acta Cryst.* D**61**, 458–464.
Miles, L. A., Dahlberg, C. M., Plescia, J., Felez, J., Kato, K. & Plow, E. F. (1991). *Biochemistry*, **30**, 1682–1691.
Mosca, M., Chimenti, D., Pratesi, F., Baldini, C., Anzilotti, C., Bombardieri, S. & Migliorini, P. (2006). *J. Rheumatol.* **33**, 695–697.
Nicholls, A., Sharp, K. A. & Honig, B. (1991). *Proteins*, **11**, 281–296.
Otwinowski, Z. & Minor, W. (1997). *Methods Enzymol.* **276**, 307–326.
Pancholi, V. (2001). *Cell. Mol. Life Sci.* **58**, 902–920.
Plow, E. F., Herren, T., Redlitz, A., Miles, L. A. & Hoover-Plow, J. L. (1995). *FASEB J.* **9**, 939–945.
Reuning, U., Magdolen, V., Wilhelm, O., Fischer, K., Lutz, V., Graeff, H. & Schmitt, M. (1998). *Int. J. Oncol.* **13**, 893–906.
Sedoris, K. C., Thomas, S. D. & Miller, D. M. (2007). *Biochemistry*, **46**, 8659–8668.
Subramanian, A. & Miller, D. M. (2000). *J. Biol. Chem.* **275**, 5958–5965.
Wang, W., Wang, L., Endoh, A., Hummelke, G., Hawks, C. L. & Hornsby, P. J. (2005). *J. Endocrinol.* **184**, 85–94.
Wedekind, J. E., Reed, G. H. & Rayment, I. (1995). *Biochemistry*, **34**, 4325–4330.
Weleber, R. G., Watzke, R. C., Shults, W. T., Trzupek, K. M., Heckenlively, J. R., Egan, R. A. & Adamus, G. (2005). *Am. J. Ophthalmol.* **139**, 780–794.
Yoneda, M., Fujii, A., Ito, A., Yokoyama, H., Nakagawa, H. & Kuriyama, M. (2007). *J. Neuroimmunol.* **185**, 195–200.
Zhang, E., Brewer, J. M., Minor, W., Carreira, L. A. & Lebioda, L. (1997). *Biochemistry*, **36**, 12526–12534.